Journal of Solid State Chemistry **147,** 573–583 (1999)
Article ID jssc.1999.8420, available online at http://www.idealibrary.com on IDEAL®

Vibrational Spectroscopic and X-Ray Diffraction Studies of Cerium Zirconium Oxides with Ce/Zr Composition Ratio = 1 Prepared by Reduction and Successive Oxidation of t'-$(Ce_{0.5}Zr_{0.5})O_2$ Phase

Takahisa Omata,* Haruo Kishimoto,* Shinya Otsuka-Yao-Matsuo,* Norikazu Ohtori,† Norimasa Umesaki‡

*Department of Materials Science and Processing, Graduate School of Engineering, Osaka University, 2-1 Yamada-oka, Suita 565-0871, Japan; †Graduate School of Science and Technology, Niigata University, Ikarashi 2-no cho, Niigata 950-2181, Japan; ‡Osaka National Research Institute (ONRI), AIST, 1-8-31 Midoriga-oka, Ikeda 563-8577, Japan

Received March 9, 1999; in revised form May 28, 1999; accepted June 1, 1999

Cerium zirconium oxides with the composition $CeZrO_4$ were prepared by oxidizing in O_2 at 873 K precursors with the composition $CeZrO_{3.5+\delta}$ ($\delta < 0.3$). The precursors were prepared by reducing the t'-$(Ce_{0.5}Zr_{0.5})O_2$ phase at $873 \leq T_{red.} \leq 1573$ K. The $CeZrO_4$ compounds together with the precursors were characterized by powder X-ray diffraction and IR and Raman spectroscopies. In the case of $1323 \leq T_{red.} \leq 1573$ K, the precursors were identified as having the pyrochlore-type $Ce_2Zr_2O_{7+2\delta}$ phase with $\delta < 0.06$. When the reduction temperature was decreased, the ordering level between Ce and Zr ions was decreased in the pyrochlore-type phase. The $CeZrO_4$ compounds obtained by oxidizing the pyrochlore-type precursors were identified as the κ-$CeZrO_4$ phase in which Ce and Zr ions are in an ordered arrangement similar to that of the pyrochlore-type structure. The space group of the κ phase was not the same as that of the pyrochlore-type structure. In the case of $T_{red.} \leq 1123$ K, cubic CaF_2-related-type $(Ce_{0.5}Zr_{0.5})O_{(3.5+\delta)/2}$ phases with $0.1 < \delta < 0.3$ were obtained. When the precursor obtained at $T_{red.} = 1123$ K was oxidized, a tetragonal phase appeared, but its Raman spectrum was different from that seen in the t' phase. This phase was identified to be a novel t'_{meta}-$(Ce_{0.5}Zr_{0.5})O_2$ phase, because it transformed into the t' phase by annealing above 1173 K under an O_2 atmosphere. When the precursor obtained at $T_{red.} = 873$ K was oxidized, the t'-$(Ce_{0.5}Zr_{0.5})O_2$ phase identical to the starting sample appeared. The structural difference between t'_{meta} and t' phases was estimated to be in their oxygen parameter, z, for the 4d site in the space group of $P4_2/nmc$. The oxygen parameter for the t'_{meta} phase is closer to 0.25 than that for t' phase. It was shown that the temperature and holding time for precursor preparation and the oxygen content δ are important factors for the structure of the reoxidized $CeZrO_4$ compound. © 1999 Academic Press

1. INTRODUCTION

CeO_2 has been used as a subcatalyst for automotive exhaust gases oxidizing harmful CO and hydrocarbons to CO_2 and H_2O gases due to its swift oxygen release property under a reducing atmosphere. With the recent increase in demand for cleaner exhaust gases, subcatalyst materials are required to improve their oxygen release property at low temperatures. Recently, it was reported that the addition of ZrO_2 into CeO_2 improved the subcatalytic property at low temperatures (1–3); however, detailed information of the phase, composition, structure, and chemical properties, remained unclear. As the intermediate composition in the CeO_2–ZrO_2 system, it is known that the tetragonal t' phase, which is believed to be a metastable phase, appears through a cation diffusionless phase transition from cubic CaF_2-type solid solutions stable above 1823 K (4). In addition to the t' phase, we reported previously that a κ-$CeZrO_4$ phase appears by oxidizing the pyrochlore-type $Ce_2Zr_2O_{7+2\delta}$ phase at 873 K (5, 6). Ce and Zr ions in the κ phase are in an ordered arrangement similar to the arrangement in the pyrochlore-type phase. We also reported that the κ phase is more metastable (7) than the t' phase and is a suitable subcatalyst material due to its excellent oxygen-releasing ability at low temperatures (5).

The formation of κ phase and its derivative phases was understood phenomenally from the schematic diagram of the phase transformation of Ce/Zr composition ratio = 1, as shown in Fig. 1. The finally formed phase strongly depends on the temperature, time, and atmosphere for the preparation of the precursor; these factors affect the oxygen content in the precursor. It is interesting to note that the κ phase appeared by oxidizing the pyrochlore-type precursor and the ordered arrangement between the cations in the pyrochlore-type precursor remained in the κ phase. In our previous studies (5, 6), the pyrochlore-type $CeZrO_{3.5+\delta}$ precursor was prepared by reducing the t' phase at 1323 K; the X-ray diffraction (XRD) characteristic of the pyrochlore structure, due to the ordered arrangement between Ce and Zr ions, showed small and diffused line. This observation

0022-4596/99 $30.00

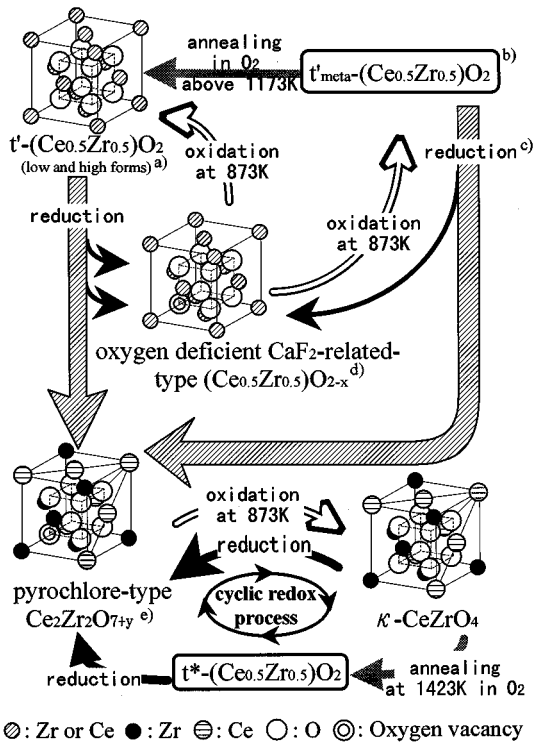

FIG. 1. Schematic diagram of the phase formation of cerium zirconium oxide with the Ce/Zr composition ratio = 1, including the cyclic redox process. The alphabetical superscripts in the figure denote the following: (a) The existence of low- and high-temperature forms of the t' phase was suggested in Ref. 7. (b) The phase formation pathways via t'_{meta}-$(Ce_{0.5}Zr_{0.5})O_2$ were discovered in the present study. (c) The formation of the pyrochlore-type phase by reducing the t'_{meta} phase was not confirmed. (d) Oxygen vacancies in the $(Ce_{0.5}Zr_{0.5})O_{2-x}$ with a CaF_2-related-type structure may be randomly distributed. (e) Ce, Zr, and oxygen vacancies were in an ordered arrangement in the pyrochlore-type phase.

was attributed to the existence of the antiphase domain boundaries; in other words, Ce and Zr ions in the pyrochlore-type phase were not ordered completely.

In the present study, we focused on the temperature for preparing precursor $CeZrO_{3.5+\delta}$, i.e., the reducing temperature, $T_{red.}$, of the starting t'-$(Ce_{0.5}Zr_{0.5})O_2$ phase, based on the following expectations: (i) At high reducing temperatures of the starting t' phase, a completely cation-ordered pyrochlore-type $Ce_2Zr_2O_{7+2\delta}$ must be prepared. If possible, the typical κ phase, in which Ce and Zr ions are completely ordered, must be prepared by oxidizing that pyrochlore-type phase. (ii) At low reducing temperatures, a cation-disordered precursor phase is expected to appear. (iii) The oxidation of the cation-disordered precursor phase may give us a new phase with composition $CeZrO_4$. From these viewpoints, various precursors with composition $CeZrO_{3.5+\delta}$ were prepared by reducing the starting t'-$(Ce_{0.5}Zr_{0.5})O_2$ phase at various temperatures.

By oxidizing these precursors at 873 K under an O_2 atmosphere, $CeZrO_4$ compounds were prepared. The oxidized phases, together with the precursor phases, were characterized from the structural viewpoints of the ordering level between Ce and Zr ions and the displacement of oxygen ions by powder XRD and IR and Raman spectroscopies. Based on the results, the structures of the precursor and the oxidized phase were examined as a function of the temperature for precursor preparation, $T_{red.}$. For the case of the reoxidation of the cation-disordered precursor obtained at $T_{red.} = 1123$ K, a novel tetragonal t'-related phase was obtained. Because the phase was transformed into the t' phase by annealing under O_2 atmosphere above 1173 K, the phase was concluded to be more metastable than the t' phase; the t'-related phase was named as the t'_{meta} phase.

2. EXPERIMENTAL

2.1. EGA Analysis

The oxygen content of the reduced samples, i.e., precursors, was considered to be one of the important factors for determining the structure and properties of reoxidized $CeZrO_4$. In this study, the starting sample was reduced in an apparatus for evolved-oxygen gas analysis (EGA). The oxygen atoms released by the samples during the heating reduction run can be monitored by EGA; this enabled us to obtain the δ value of reduced $CeZrO_{3.5+\delta}$. The EGA apparatus consists of a closed-system oxygen gas analyzer including an electrochemical oxygen pump: Pt, air/ZrO_2(+CaO) electrolyte/Ar, Pt. The oxygen analyzer developed by one of the present authors enables measurements with much higher sensitivity and therefore uses smaller amounts of samples than such conventional techniques as gas chromatography–mass spectrometry or mass thermobalance. Details regarding the experimental principle of EGA, the oxygen analyzer, and the procedures for determining the amount of oxygen released have been described in earlier papers (6, 8, 9).

2.2. Preparation of Starting t' Phase and Reduced and Reoxidized Samples

Starting t'-$(Ce_{0.5}Zr_{0.5})O_2$ was prepared by the conventional ceramic method as follows. Powdered raw materials CeO_2 (Na, <100 ppm; Fe, <10 ppm) and ZrO_2 (HfO_2, 3.8 mass%; Na, <100 ppm; Fe, <100 ppm), which were supplied by Santoku Kinzoku Kogyo Co., Ltd., were thoroughly mixed in a molar ratio of 1:1 using a ball mill, and pressed into 17-mm-diameter disks under 100 MPa. The disks were sintered in air at 1923 K for 50 h to attain a single phase with a cubic CaF_2-type structure; when they were cooled by cutting the electric power off in the furnace, the phase transformed to single t'-$(Ce_{0.5}Zr_{0.5})O_2$ phase.

In the case of reducing temperatures below 1373 K, the starting t' phase was reduced while monitoring oxygen atoms released using the closed-system oxygen analyzer.

Since carbon-related compounds such as CO and hydrocarbon adsorbed on the sample chamber hinder precise EGA, the sample chamber containing an alumina crucible was heated before sample loading at 1373 K for 5 h by circulating pure O_2 gas. The system was then evacuated for a few minutes and O_2 gas was reintroduced, and then the system was cooled to room temperature. The experimental procedure after this process is illustrated in Fig. 2a. After the starting t' sample of approximately 100 mg was loaded in the alumina crucible and O_2 gas was introduced, the sample was annealed at 873 K for 5 h to control the oxygen content in it; its composition after the annealing was regarded as stoichiometric $(Ce_{0.5}Zr_{0.5})O_2$. The system was evacuated after being cooled to 373 K in O_2 gas, and then the $Ar + 1\%H_2$ gas mixture was introduced and circulated.

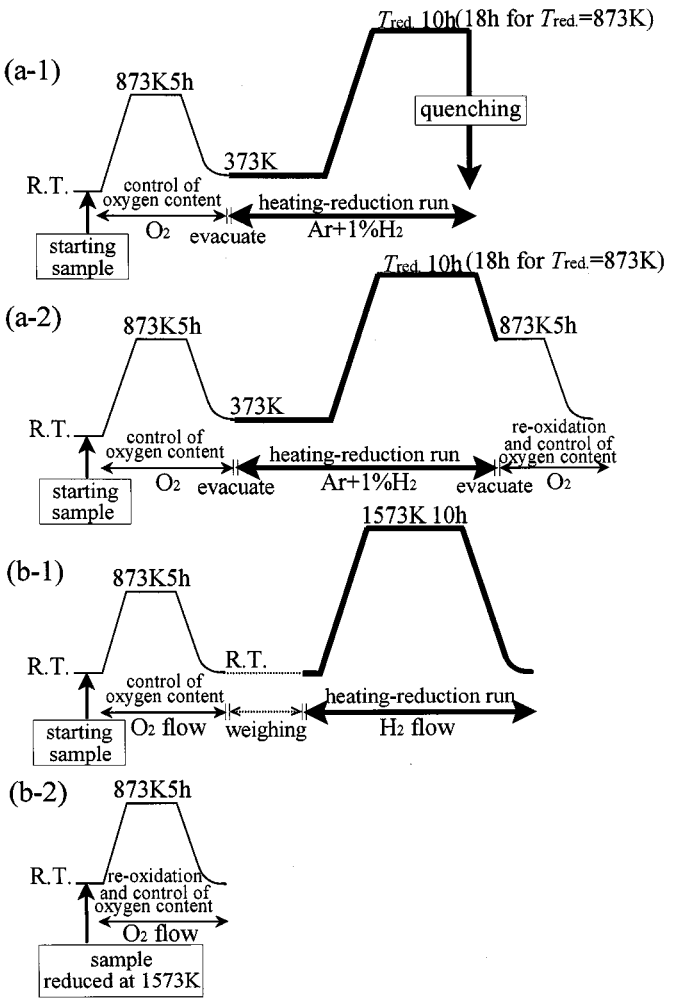

FIG. 2. Schematic description of the temperature-time patterns for obtaining (a1) reduced $CeZrO_{3.5+\delta}$ at reduction temperature $T_{red.} \leq 1373$ K, (a2) reoxidized $CeZrO_4$ with $T_{red.} \leq 1373$ K, (b1) reduced $CeZrO_{3.5+\delta}$ with $T_{red.} = 1573$ K, and (b2) reoxidized $CeZrO_4$ with $T_{red.} = 1573$ K. All heating and cooling rates are 2 K min^{-1}.

Ten hours after the potentiostatic operation with four leads, the base current, $I_\infty(t)$, became sufficiently small. The heating–reduction run was started by heating the sample at a rate of 2 K min^{-1} to the appropriate temperatures $T_{red.}$ of 1373, 1323, 1123, 973, and 873 K. During the heating, the sample was reduced with oxygen being released. After holding for 10 h at the $T_{red.}$, the sample chamber was quenched by ice water and the sample was unloaded as a reduced sample. For the case of $T_{red.} = 873$ K, the sample was held at $T_{red.}$ for 18 h. To obtain reoxidized phases (in Fig. 2a2), after the sample was cooled to 873 K, the system was evacuated, and O_2 gas was introduced. The sample could be oxidized again to its initial composition of $CeZrO_4$; it was confirmed by a separate EGA experiment that the oxygen content in the reoxidized samples is equivalent to that in the samples before reduction. After cooling the sample to 373 K, the reoxidized sample was unloaded.

The samples reduced at $T_{red.}$ of 1573 K were prepared by the following procedure. The starting t' pellet was crushed into grains and was then annealed once in O_2 flow at 873 K for 5 h to control the oxygen content. After the sample was weighed, it was loaded in an alumina tube equipped in a conventional electric furnace. The sample was heated to 1573 K and held there for 10 h, and then it was cooled to room temperature in the furnace. In this heating–reduction run, pure H_2 gas was introduced into the alumina tube at a flow rate of 100 cm^3 min^{-1}. The reduced sample was unloaded and weighed. The δ value for this sample was determined by the change in sample weight; the sample weight changed from 1.6809 g before reduction to 1.6371 g after reduction. Both heating and cooling rates were 2 K min^{-1}. The sample reduced at 1573 K was reoxidized at 873 K for 5 h in pure O_2 gas flow (in Fig. 2b2).

2.3. X-Ray Powder Diffraction and Vibrational Spectroscopy

The precursor and reoxidized samples obtained were identified by the X-ray powder diffraction method (Cu$K\alpha$ radiation, using curved graphite $K\beta$ filter, 40 kV–200 mA) (MXP18, MAC Science, Yokohama, Japan). Lattice parameters were calculated using the least squares procedure (code RSLC) from 7 to 11 diffraction peaks for a cubic system or 10 or 11 diffraction peaks for a tetragonal system at 2θ above 45°. High-purity silicon powder was mixed with the samples as an internal standard.

The Raman spectra of the powdered samples were recorded with a Raman spectrometer with a triple monochromator and a liquid-N_2-cooled CCD detector (Ramanor, T64000, Atago-Jobin Yvon, Tokyo, Japan) or with a double monochromator and photomultiplier detector (JASCO, NR1100, Nihon Bunko, Tokyo, Japan). The spectra were excited with an Ar ion laser operating at 514.5 nm wavelength and 5 to 100 mW power (Innova 300 or 90C,

Coherent, Santa Clara, CA). Infrared absorption spectra were recorded with a Fourier transform infrared spectrometer (FT/IR-610V, JASCO, Nihon Bunko, Tokyo, Japan). The finely ground samples were in the form of powder dispersed in cesium iodide (CsI) disks.

3. RESULTS

3.1. Starting Sample and Its EGA Results

The powder X-ray diffraction pattern and the Raman spectrum of the starting sample completely agreed with those of tetragonal t'-$(Ce_{0.5}Zr_{0.5})O_2$ with a space group of $P4_2/nmc$ (6, 10, 11). Thus, the starting $(Ce_{0.5}Zr_{0.5})O_2$ sample was identified to have the t'-$(Ce_{0.5}Zr_{0.5})O_2$ phase.

Figure 3 shows the oxygen evolution behavior (EGA results) for samples with various $T_{red.}$, i.e., the J_O–T–t curves, which were obtained by heating-reduction runs of t'-$(Ce_{0.5}Zr_{0.5})O_2$ which was sintered at 1923 K. As seen in the curve of $T_{red.} = 1373$ K, oxygen evolution started at about 773 K under $P(H_2O)/P(H_2) = 4.2 \times 10^{-4}$ atmosphere. After the maximum evolution rate was observed at 1053 K, the rate decreased rapidly; slow and continuous evolution of a shoulder was observed above 1173 K; the evolution rapidly decreased and stopped when the temperature was held at 1373 K. In the J_O–T–t curve, on set and peak temperatures were higher than those in the curve for 35.5 mg of t'-$(Ce_{0.5}Zr_{0.5})O_2$ sintered at 1823 K (6, 12).

δ Values and reduction ratios, $Ce^{3+}/(Ce^{3+} + Ce^{4+})$, in the reduced samples of $CeZrO_{3.5+\delta}$ composition with various $T_{red.}$ are summarized in Table 1. δ was increased, i.e., the reduction ratio was decreased, with decreasing $T_{red.}$.

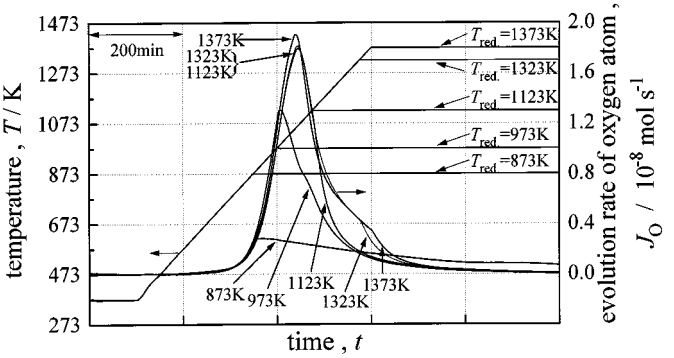

FIG. 3. J_O–T–t curves of the heating-reduction runs obtained for t'-$(Ce_{0.5}Zr_{0.5})O_2$ powder at various reducing temperatures $T_{red.} \leq 1373$ K. J_O indicates the oxygen evolution rate in mol of oxygen atom per second.

3.2. XRD Patterns and Vibrational Spectra of Precursors

The XRD patterns for precursors with the composition $CeZrO_{3.5+\delta}$ prepared at various reducing temperatures, $T_{red.}$, are shown in Fig. 4. For the precursor obtained at $T_{red.} = 1573$ K, all the diffraction peaks were indexed assuming that the phase was the pyrochlore-type $Ce_2Zr_2O_{7+2\delta}$ (13, 14). Weak diffractions with indices of all odd numbers of (*hkl*), (422), and (620) were characteristic of the pyrochlore-type phase due to the ordered arrangement

TABLE 1
Structural and Compositional Parameters for $CeZrO_{3.5+\delta}$ and $CeZrO_4$ Compounds

	Reduced $CeZrO_{3.5+\delta}$ (precursor)						Reoxidized $CeZrO_4$				
Reduction temperature T_{red} (K)	Reduction ratio[a] $Ce^{3+}/(Ce^{3+}+Ce^{4+})$	δ value[a]	Crystal system	Phase	Lattice parameter[b] (nm)	Unit cell volume[b] V (nm^3)	Crystal system	Phase	Lattice parameter[b,c] (nm)	c_F/a_F ratio	Unit cell volume[b] V (nm^3)
1573	0.96	0.002	Cubic	Pyrochlore	$a_0 = 1.07414(3)$	1.2393(1)	Cubic	κ	$a_0 = 1.05250(1)$	—	1.1659(1)
1373	0.900	0.050	Cubic	Pyrochlore	$a_0 = 1.07338(4)$	1.2367(1)	Cubic	κ	$a_0 = 1.05370(3)$	—	1.1699(1)
1323	0.888	0.056	Cubic	Pyrochlore	$a_0 = 1.07268(4)$	1.2343(2)	Cubic	κ	$a_0 = 1.05380(3)$	—	1.1703(1)
1123	0.774	0.113	Cubic	CaF_2-related	$a_0 = 0.53503(4)$	0.15316(2)	Tetragonal	t'_{meta}	$a_F = 0.52571(3)$	1.0082	0.14649(2)
						($8V = 1.2252$)			$c_F = 0.53002(2)$		($8V = 1.1719$)
973	0.580	0.210	Cubic	CaF_2-related	$a_0 = 0.53322(1)$	0.15160(1)	Tetragonal	t'_{meta}	$a_F = 0.52583(2)$	1.0088	0.14667(1)
						($8V = 1.2128$)			$c_F = 0.53046(2)$		($8V = 1.1734$)
873	0.406	0.297	Cubic	CaF_2-related	$a_0 = 0.53218(2)$	0.15072(2)	Tetragonal	t'	$a_F = 0.52598(3)$	1.0091	0.14684(2)
						($8V = 1.2058$)			$c_F = 0.53077(2)$		($8V = 1.1747$)
						Starting sample	Tetragonal	t'	$a_F = 0.52605(2)$	1.0091	0.14689(1)
									$c_F = 0.53082(2)$		$8V = 1.1751$

[a] The reduction ratio and the δ value for the reduced $CeZrO_{3.5+\delta}$ obtained at $T_{red} = 1573$ K were determined from the change in the sample weight before and after the reduction.

[b] The number in the parentheses shows the standard deviation estimated in the last digit.

[c] The lattice parameters for the tetragonal phases of t' and t'_{meta} were adopted assuming a pseudofluorite unit cell. Actual lattice parameters a_0 and c_0 of the dimolecular unit cell based on the space group $P4_2/nmc$ were expressed by $a_0 = a_F/\sqrt{2}$ and $c_0 = c_F$, respectively.

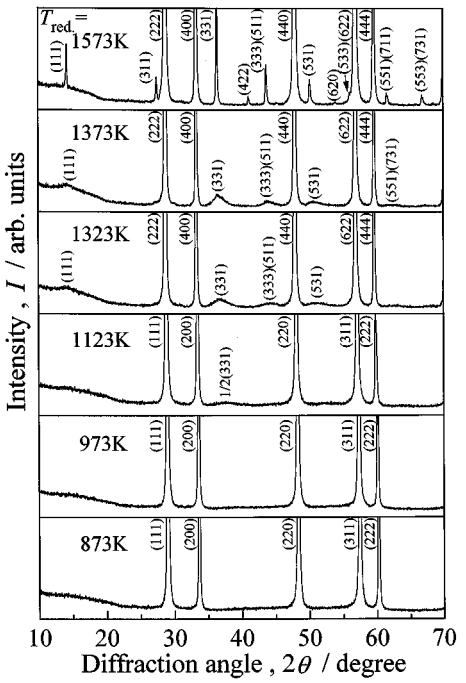

FIG. 4. Powder X-ray diffraction patterns for reduced $CeZrO_{3.5+\delta}$ compounds prepared at various reducing temperatures, $T_{red.}$.

between Ce and Zr ions. It may be concluded that Ce^{3+} and Zr^{4+} ions completely ordered along the $\langle 110 \rangle$ direction in the pyrochlore-type precursor with $T_{red.} = 1573$ K, because the characteristic peaks were clearly observed. For the precursors obtained at $T_{red.} = 1373$ and 1323 K, diffractions characteristic of the pyrochlore-type phase were broadened; some of these diffractions could not be observed. However, diffractions with indices of (111), (331), (333), (511), and (531) were clearly observed; these precursors may be also identified to have the pyrochlore-type phase. Such a broadening of the diffractions characteristic of the pyrochlore-type phase is attributable to the existence of the antiphase domain boundaries lying parallel to the {112} as well as the case of $Gd_2Zr_2O_7$ pyrochlore (15, 16). The antiphase domain boundaries break the ordered arrangement between the cations. Therefore, the ordering level of Ce and Zr ions in the pyrochlore-type precursor decreased with decreasing reducing temperature, $T_{red.}$.

For the precursor obtained at $T_{red.} = 1123$ K, diffractions characteristic of the pyrochlore phase completely vanished except for the extremely broadened 1/2(311) diffraction. Based on the following IR results, the sample obtained at $T_{red.} = 1123$ K was identified to have an oxygen-deficient CaF_2-related $(Ce_{0.5}Zr_{0.5})O_{2-x}$ $[(Ce_{0.5}Zr_{0.5})O_{(3.5+\delta)/2}]$ phase, in which cations might be completely disordered. For the precursors obtained at $T_{red.} = 973$ and 873 K, only the fundamental diffractions of the cubic CaF_2-type structure were observed; these indicate that the phase is the same as that of the precursor obtained at $T_{red.} = 1123$ K.

Lattice parameters and unit cell volume, together with the oxygen content for the precursors, are summarized in Table 1. For both the pyrochlore-type phase and the CaF_2-related phase, the lattice parameter decreased with decreasing reducing temperature. The oxygen content, δ, for the precursors increased with decreasing reducing temperature. The larger δ value corresponds to the larger Ce^{4+} content; the smaller lattice parameter for the precursor prepared at a lower reducing temperature may be caused by the higher concentration of Ce^{4+} whose ionic radius is smaller than that of Ce^{3+}.

Figure 5 shows the IR absorption spectra for the precursors. For the sample obtained at $T_{red.} = 1573$ K, one absorption doublet peaking at 511 and 591 cm^{-1} and a strong absorption band at regions below 400 cm^{-1} were observed. These spectral features agreed with the reported IR spectra for various rare-earth zirconates and hafnates ($Ln_2Zr_2O_7$ and $Ln_2Hf_2O_7$; Ln, rare-earth elements) with a pyrochlore structure (17–20). For the samples obtained at $T_{red.} = 1373$ and 1323 K, the strong absorption doublet was broadened, but still clearly observed. The precursor obtained at $T_{red.} \geq 1323$ K was identified to have the pyrochlore-type phase. For the samples obtained at $T_{red.} \leq 1123$ K, a weak and broad absorption band at ~ 580 cm^{-1} and a strong absorption band at regions below 400 cm^{-1} were detected; the doublet characteristic of the pyrochlore phase could not be observed. The phase in the samples obtained at

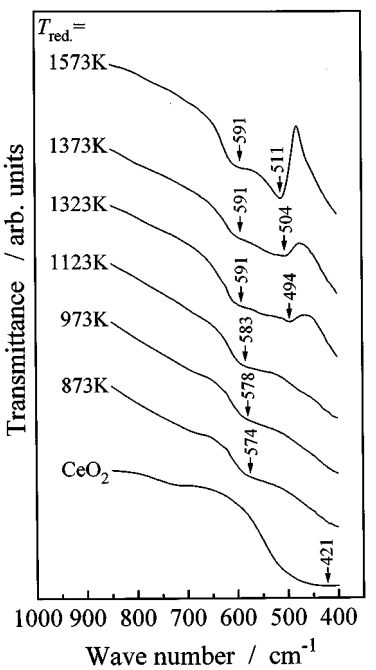

FIG. 5. IR absorption spectra for reduced $CeZrO_{3.5+\delta}$ compounds prepared at various reducing temperatures, $T_{red.}$.

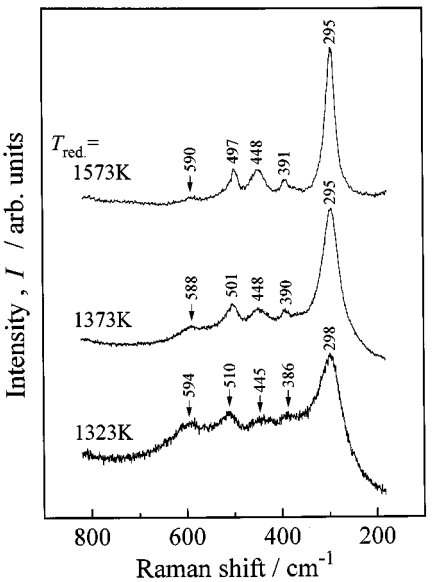

FIG. 6. Raman spectra for reduced $CeZrO_{3.5+\delta}$ compounds prepared at various reducing temperatures, $T_{red.}$. The spectra for the compounds obtained at $T_{red.} \leq 1123$ K could not be recorded because of their deep coloration in visible light.

$T_{red.} \leq 1123$ K could not be identified as a pyrochlore-type phase. However, for the simple CaF_2-type phase, only one strong absorption band at $\sim 400\ cm^{-1}$ is allowed (21) in its IR spectra, as observed for CeO_2 (Fig. 5). Therefore, the precursor obtained at $T_{red.} \leq 1123$ K was identified to have an oxygen-deficient CaF_2-related phase, in which the constituent cations may be randomly mixed.

Figure 6 shows the Raman spectra for the precursors obtained at $T_{red.} \leq 1323$ K. The Raman spectra for the precursors obtained at $T_{red.} \leq 1123$ K could not be recorded because of their deep coloration in visible light. Although we attempted recording a spectrum using an FT–Raman spectrometer with YAG laser excitation of 1.06 μm, the spectrum could not be obtained due to thermal damage by the near-infrared excitation beam. For the precursor obtained at $T_{red.} = 1573$ K, a strong peak at 295 cm^{-1} and four weak peaks at 391, 448, 497, and 590 cm^{-1} were observed. Their peak positions and relative intensities agreed well with those observed for pyrochlore-type $La_2Zr_2O_7$ and $Nd_2Zr_2O_7$ reported by Vandenborre and coworkers (18–20). For the precursors obtained at $T_{red.} = 1373$ and 1323 K, the spectra were almost identical with that for the precursor obtained at $T_{red.} = 1573$ K. Therefore, all the precursors obtained at $T_{red.} \geq 1323$ K were identified to have the pyrochlore-type $Ce_2Zr_2O_{7+2\delta}$ phase. The small broadening of the Raman peaks for the precursors obtained at $T_{red.} = 1373$ and 1323 K may be due to the antiphase domain boundaries in the pyrochlore-type phase. Distinct peak shift and/or changes in the relative intensity could not be observed in the spectra for the three pyrochlore-type precursors.

3.3. *XRD Patterns and Vibrational Spectra of Reoxidized Samples*

Figure 7 shows the XRD patterns for the reoxidized samples. For the sample prepared from the pyrochlore-type precursors obtained at $T_{red.} = 1573$ K, the XRD pattern was distinctly different from that of the t'-$(Ce_{0.5}Zr_{0.5})O_2$ phase, but very similar to that of its precursor having pyrochlore-type phase; fundamental diffractions for the CaF_2-type structure and sharp diffractions characteristic of the ordered arrangement of constituent cations with indices of all odd numbers of (*hkl*) and (422) were clearly observed. Thus, the reoxidized phase obtained at $T_{red.} = 1573$ K was identified as the κ-$CeZrO_4$ phase (5, 6), in which Ce and Zr ions retain their ordered arrangement in the precursor with the pyrochlore-type phase. In addition to these diffractions, many small superlattice diffractions, marked by asterisks in Fig. 7, were observed; all of these diffractions were also indexed, assuming a cubic system with $a_0 = 1.05250$ nm, as shown in Fig. 8. However, these small superlattice diffractions are forbidden for the space group of $Fd3m$, which is the same as the space group for the pyrochlore-type structure.

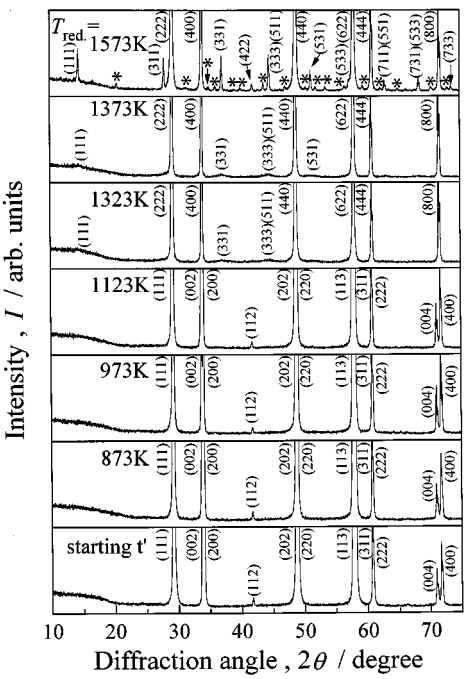

FIG. 7. Powder X-ray diffraction patterns for $CeZrO_4$ compounds prepared by reoxidation of precursor $CeZrO_{3.5+\delta}$ in pure O_2 gas at atmospheric pressure and 873 K. Diffraction peaks marked by asterisks in the pattern of the sample obtained at $T_{red.} = 1573$ K can be indexed based on the cubic system with a lattice parameter of 1.05250 nm. However, these are forbidden diffractions assuming a space group of $Fd3m$.

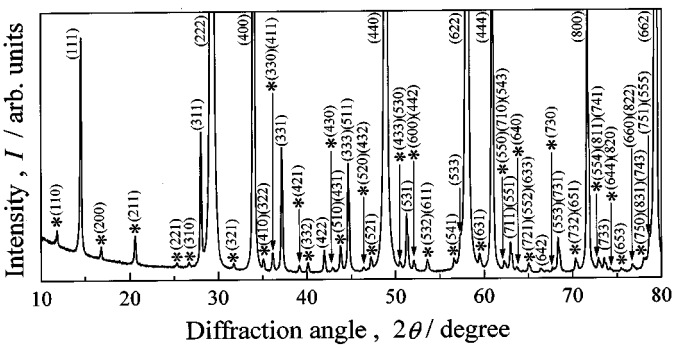

FIG. 8. Powder X-ray diffraction pattern for the cubic κ-$CeZrO_4$ phase obtained by reoxidation of the precursor pyrochlore phase with composition $CeZrO_{3.52}$ ($Ce_2Zr_2O_{7.04}$; $T_{red.} = 1573$ K). Diffraction peaks marked by asterisks were not observed in the XRD pattern for the precursor pyrochlore phase and are forbidden for the space group of *Fd3m*.

Therefore, the κ-$CeZrO_4$ phase belongs to the cubic system, but its space group has lower symmetry than *Fd3m*. The small superlattice diffractions could not be observed in previously reported XRD results for the κ phase (5, 6) which was prepared by reducing the t' phase at 1323 K. We consider the κ phase obtained at $T_{red.} = 1573$ K in the present study to be a typical κ phase. For the reoxidized samples obtained at $T_{red.} = 1373$ and 1323 K, diffractions with indices of (311), (422), (533), (711), (551), (731), (533), and (733) and small superlattice diffractions could not be observed. Because diffractions with indices of (111), (331), (333), (511), and (531) were clearly observed, the samples were identified as a kind of κ-$CeZrO_4$ phase. The ordering level of the cations in κ-$CeZrO_4$ phase for the samples obtained at $T_{red.} = 1373$ and 1323 K was considered to be lower than that in the phase for the sample obtained at $T_{red.} = 1573$ K, because diffractions with indices of (111), (331), (333), (511), and (531) were broadened due to antiphase domain boundaries. The previously reported κ phase may correspond to the phase for the samples obtained at $T_{red.} = 1373$ or 1323 K in the present study.

The XRD patterns for samples obtained at $T_{red.} \leq 1123$ K drastically differed from those of the samples obtained at $T_{red.} \leq 1323$ K. The diffractions with indices of (400) and (004) were clearly split. The (112) diffraction due to displacement of oxygen in the CaF_2-related lattice was clearly observed. The samples were identified to have the tetragonal t' or its related phase, because the diffraction patterns agreed with that of the starting t'-$(Ce_{0.5}Zr_{0.5})O_2$ phase.

Table 1 shows lattice parameters and unit cell volumes for the reoxidized phases. For tetragonal phases, lattice parameters expressed by a_F and c_F are adopted based on the pseudofluorite cell, although $a_0 = a_F/\sqrt{2}$ and $c_0 = c_F$ are actual lattice parameters for the space group of $P4_2/nmc$ with a dimolecular cell. The unit cell volume increased with decreasing $T_{red.}$. The c_F/a_F ratio for the tetragonal phases increased with decreasing $T_{red.}$; lattice parameters and the c_F/a_F ratio of the phase for the sample obtained at $T_{red.} = 873$ K agreed well with those of starting t'-$(Ce_{0.5}Zr_{0.5})O_2$.

Figure 9 shows the IR absorption spectra of the reoxidized phases. In the spectrum of the κ-$CeZrO_4$ phase obtained at $T_{red.} = 1573$ K, a sharp absorption band at 735 cm^{-1} and at least seven complex bands at regions below 600 cm^{-1} were observed. This spectrum is considered to be the IR spectrum for the typical κ-$CeZrO_4$ phase. For the κ-$CeZrO_4$ phase obtained at $T_{red.} = 1373$ and 1323 K, the absorption bands were broadened compared to the bands for the κ phase obtained at $T_{red.} = 1573$ K. For the tetragonal samples obtained at $T_{red.} \leq 1123$ K, three bands at 658, 576, and ~ 410 cm^{-1} were observed; no distinct differences in the IR spectra could be detected between these tetragonal phases and the starting t' phase.

Figures 10a and 10b show the Raman spectra of the κ and the tetragonal phases, respectively. Many peaks that accompany the three strong peaks at 271, 437, and 598 cm^{-1} were observed in the spectrum for the typical κ-$CeZrO_4$ phase obtained at $T_{red.} = 1573$ K; this Raman spectrum with many peaks is characteristic of the κ-$CeZrO_4$ phase. The spectrum was distinctly different from that of the precursor pyrochlore-type phase which belongs to the space group of *Fd3m*. The κ phase might belong to a space group having

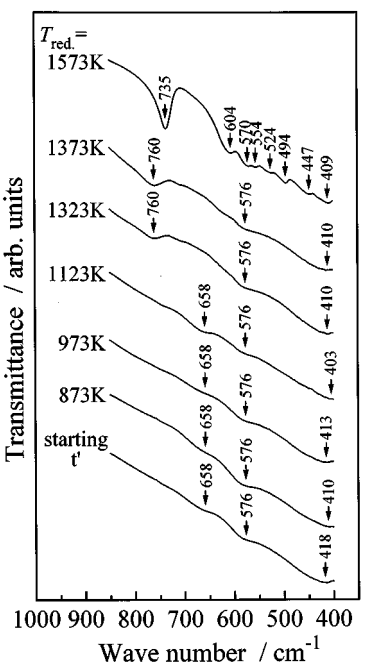

FIG. 9. IR absorption spectra for reoxidized $CeZrO_4$ compounds prepared by oxidation of precursor $CeZrO_{3.5+\delta}$ in pure O_2 gas at atmospheric pressure and 873 K.

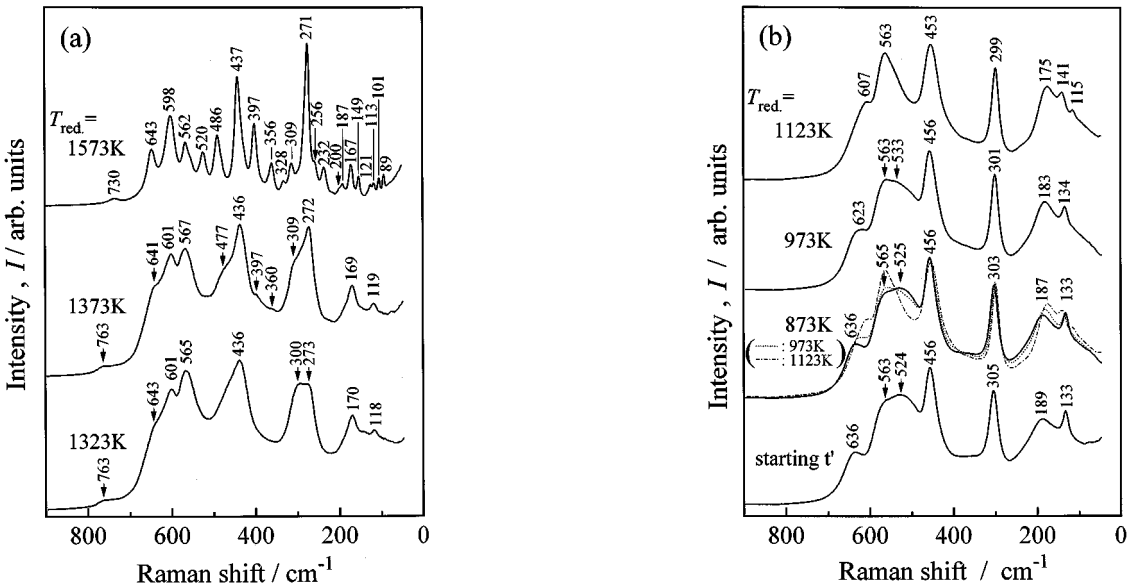

FIG. 10. Raman spectra for $CeZrO_4$ compounds prepared by reoxidation of precursor $CeZrO_{3.5+\delta}$ in pure O_2 gas at atmospheric pressure and 873 K. (a) Cubic κ-$CeZrO_4$ phases obtained at $T_{red.} \geq 1323$ K and (b) tetragonal $(Ce_{0.5}Zr_{0.5})O_2$ phases obtained at $T_{red.} \leq 1123$ K.

a lower symmetry than *Fd3m*. For the κ-$CeZrO_4$ phases obtained at $T_{red.} = 1373$ and 1323 K, the peaks became broader than those of the phase obtained at $T_{red.} = 1573$ K; positions and relative intensities for some of the peaks were distinctly different from those of the κ phase obtained at $T_{red.} = 1573$ K. However, three strong peaks at around 270, 440, and 600 cm^{-1}, which were characteristic of the κ phase, were clearly observed. Therefore, the phases obtained at $T_{red.} = 1373$ and 1323 K could be identified as the κ phase also by Raman spectroscopy. Since the intensity of Raman peaks in solids oxide is mainly affected by oxygen atoms with high polarizability, we inferred that the difference in the relative intensities of Raman bands among the three κ phases may be due to the difference in the displacement of oxygen in these phases.

The Raman spectrum for the reoxidized phase obtained at $T_{red.} = 873$ K was identical to that for the starting t'-$(Ce_{0.5}Zr_{0.5})O_2$ phase; the reoxidized sample obtained at $T_{red.} = 873$ K was identified to have the t' phase. The apparent intensity ratio of the peaks around 530 and 560 cm^{-1}, I_{530}/I_{560}, decreased with increasing $T_{red.}$; the peak around 530 cm^{-1} became very small and could not be isolated from the spectrum of the phase obtained at $T_{red.} = 1123$ K, although the intensity of the peaks around 530 cm^{-1} was comparable to that of the peak around 560 cm^{-1} for the phase obtained at $T_{red.} = 873$ K. Therefore, the phase obtained at $T_{red.} = 1123$ K was distinguished from the t' phase and identified as a novel t' related phase. The t'-related and t' phases were also distinguished by the electrical conductivity measurements by the dc four-probe technique using Pt-black electrodes. The electrical conductivity and temperature dependence of the t'-related phase under O_2 atmosphere was clearly different from that of the t' phase. The electrical conductivity at 973 K of the t'-related phase was 7.5 times higher than that of the t' phase. After heating above 1173 K, the electrical conductivity and temperature dependence of the t'-related phase completely agreed with that of the t' phase; the Raman spectrum showed that the t'-related phase transformed into the t' phase by heating above 1173 K under an O_2 atmosphere. Therefore, it is confirmed that the t'-related phase is more metastable than the t' phase; the t'-related phase was named as the t'_{meta} phase. The change in the apparent intensity ratio may be due to the shift of the peak positions for 530 and 560 cm^{-1} bands. The phase obtained at $T_{red.} = 973$ K may be identified as a kind of t'_{meta} phase, because its Raman spectrum was distinctly different from that of the t' phase but was similar to that of the t'_{meta} phase. The t'_{meta} phase obtained at $T_{red.} = 1123$ K is assumed to be the most typical t'_{meta}-$(Ce_{0.5}Zr_{0.5})O_2$ phase because its Raman spectrum is the most characteristic among the samples obtained in the present study.

4. DISCUSSION

4.1. Structural Features of κ-$CeZrO_4$ and t'_{meta}-$(Ce_{0.5}Zr_{0.5})O_2$ Phases

We have successfully prepared typical κ-$CeZrO_4$ and t'_{meta}-$(Ce_{0.5}Zr_{0.5})O_2$ phases. In this subsection, detailed structural features and their relationships with the thermodynamic stability of these phases are discussed.

First, the structure of κ-$CeZrO_4$ is discussed. Based on the CaF_2-type structure, there is an empty quasi-anion site

in the precursor pyrochlore-type lattice, i.e., the 8*b* site in the space group of *Fd*3*m* (22). One can estimate that the κ-$CeZrO_4$ phase has the oxygen excess pyrochlore-type structure (23) in which excess oxygen atoms occupy the quasi-anion site. The structural model for the κ phase is satisfactory in qualitative terms. However, it is not strictly correct because the observed XRD diffractions marked by asterisks in Figs. 7 and 8 are forbidden and only seven Raman active modes are allowed assuming the space group of *Fd*3*m*. Assuming that the κ phase belongs to the cubic system with $a_0 = 1.05250$ nm, $P2_13$, $P23$, and $P\bar{4}3m$ are the possible space groups taking into account the conditions that limit the possible XRD diffractions and reproduce the ordered arrangement between Ce and Zr ions along the $\langle 110 \rangle$ direction in the unit cell. Rietveld analysis based on the above assumption showed that $P2_13$ is the most probable space group; detailed structural parameters for κ-$CeZrO_4$ with $P2_13$ will be reported in a separate paper (24). The structural features concerning the local environment of cations are briefly stated in the present paper. Both Zr^{4+} and Ce^{4+} ions in the κ phase are surrounded by eight oxygen ions. It is well known that the Zr^{4+} ion in fluorite-related type oxide solids does not prefer cubic eightfold coordination; in monoclinic ZrO_2 phase, Zr^{4+} ion has sevenfold coordination (25). Therefore, such a compulsive eightfold coordination of the Zr^{4+} ion in the κ phase, in addition to the ordered arrangement between Zr^{4+} and Ce^{4+} ions, may be due to the fact that the κ-$CeZrO_4$ phase is more thermodynamically unstable than the t'-$(Ce_{0.5}Zr_{0.5})O_2$ phase (7).

Second, we discuss the structure of the t'_{meta}-$(Ce_{0.5}Zr_{0.5})O_2$ phase. Although the lattice parameter of the t'_{meta} phase (in Table 1) was slightly smaller than that of the t' phase, the XRD pattern of the t'_{meta} phase was almost identical to that of the t' phase. This means that the t'_{meta} phase has approximately the same structure as that of the t' phase. Consequently, it is considered that the t'_{meta} phase belongs to the space group of $P4_2/nmc$ and the atomic coordinates of cations and oxygen are (0, 0, 0) of the 2*e* site and (0, 0.5, *z*) with $z < 0.25$ of the 4*d* site, respectively. The difference between the t'_{meta} and t' phases is inferred to lie in their oxygen parameter, *z*, due to the following reasons. Figure 11 shows the plot of the oxygen parameter, *z*, vs the c_F/a_F ratio assuming a pseudofluorite unit cell for tetragonal *t*, *t*′, and *t*″ phases with various ZrO_2-based compositions. The plotted oxygen parameters were previously reported in data obtained by the neutron diffraction technique (26–33). As shown in the figure, it is clearly observed that the deviation of the oxygen parameter, *z*, from 0.25 increases continuously with increasing c_F/a_F ratio. Such a relationship between c_F/a_F ratio and oxygen parameter is independent of the species of the dopant cations or the composition. Based on this relationship, the oxygen parameters are estimated to be 0.218 and 0.220 for the starting

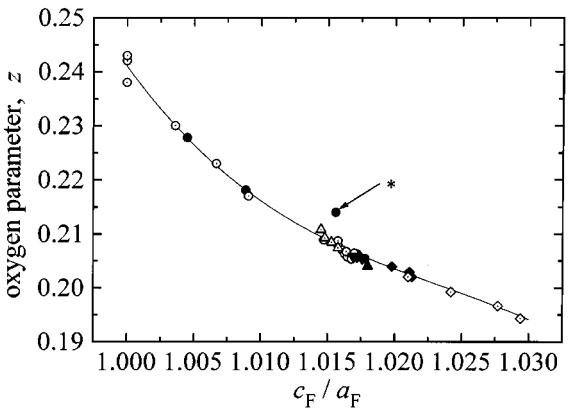

FIG. 11. Plot of the oxygen parameter, *z*, vs the length ratio of c_F to a_F, c_F/a_F, for the tetragonal *t*, *t*′, and *t*″ phases belonging the space group of $P4_2/nmc$ appearing in ZrO_2-based systems. ▲, ZrO_2 (26); ○, ZrO_2–$YO_{1.5}$ system (27)–(31); ●, ZrO_2–CeO_2 system (32, 33); △, ZrO_2–$YO_{1.5}$–CeO_2 system (31); ▼, ZrO_2–$YO_{1.5}$–GeO_2 system (31), ◇, ZrO_2–$YO_{1.5}$–TiO_2 system (31); and ◆, ZrO_2–$YO_{1.5}$–SnO_2 system (31). a_F and c_F are the lattice parameters assuming a pseudofluorite unit cell for these tetragonal phases. Actual lattice parameters, a_0 and c_0, based on the $P4_2/nmc$ are expressed as $a_0 = a_F/\sqrt{2}$ and $c_0 = c_F$, respectively. The point that deviated largely from the curve (marked by an asterisk) represents the *t*-$(Ce_{0.1}Zr_{0.9})O_2$ phase. Because its structural data were refined under the coexistence of a monoclinic phase, the oxygen parameter and the lattice parameters may be inaccurate.

t'-$(Ce_{0.5}Zr_{0.5})O_2$ and t'_{meta}-$(Ce_{0.5}Zr_{0.5})O_2$ with $T_{red.} = 1123$ K, respectively. Since the intensity of Raman peaks in solid oxides is mainly affected by oxygen atoms with high polarizability, it is probable that the difference in the intensity ratio of I_{530}/I_{560} and the peak positions between the Raman spectra of t'_{meta} and t' phases are due to the difference in the oxygen parameters between the two phases. This structural difference in the oxygen parameters between t'_{meta} and t' phases gives us a clue to why the t'_{meta} phase is more unstable than the t' phase. The oxygen coordination number of cations is changed from 8 to 4 + 4 upon increasing the deviation in oxygen parameter from 0.25. In the t'_{meta}-$(Ce_{0.5}Zr_{0.5})O_2$ phase, the oxygen parameter estimated to be 0.220 is closer to 0.25 than that of the t' phase (0.218). The coordination state of both Zr^{4+} and Ce^{4+} ions is regarded to be closer to eightfold in the t'_{meta} phase than that in the t' phase. The Zr^{4+} ion does not prefer eightfold coordination as described above. It is possible that the difference in the coordination states of Zr^{4+} ion between t'_{meta} and t' phases influences their thermodynamic stability, even if the difference is very small.

We have reported another t'-related phase which is called the t^* phase. The intensity ratio of 560 and 530 cm^{-1} peaks in the Raman spectrum of the t^*-$(Ce_{0.5}Zr_{0.5})O_2$ phase (Fig. 5 in Ref. 6) is similar to that of the t'_{meta}-$(Ce_{0.5}Zr_{0.5})O_2$ phase obtained at $T_{red.} = 1123$ K. However, all the observed Raman shift for individual peaks in the t^* phase did not deviate from that for corresponding peaks in the t'

phase. Therefore the t^* phase could be distinguished from t'_{meta}-phase.

4.2. Factors Affecting the Structure of Precursors and Reoxidized Phases

The crystal structure of the precursor phases depends on the reducing temperature of the starting t'-$(Ce_{0.5}Zr_{0.5})O_2$ phase. For instance, in the case of $T_{red.} \geq 1323$ K, the structure of precursors was of the pyrochlore type, but for $T_{red.} \leq 1123$ K it was of the oxygen-deficient CaF_2-related type. Not only the oxygen release but also the atomic diffusion of Ce and Zr has to be carried out through the reduction from the starting t'-$(Ce_{0.5}Zr_{0.5})O_2$ phase to the pyrochlore-type $Ce_2Zr_2O_{7+2\delta}$ phase, because Ce and Zr ions are randomly distributed in the t' phase but in ordered arrangement in the pyrochlore-type phase. Since atomic diffusion occurs rapidly at a high temperature, it can be easily understood that the pyrochlore-type $Ce_2Zr_2O_{7+2\delta}$ appears only at a high reducing temperature. Therefore, the atomic diffusion of cations promoted by temperature is one of the most important factors for determining the structure of precursors; of course the reduction time is the important factor. The reduction ratio, i.e., the oxygen content of the precursor, is considered to be an additional important factor for determining the structure of the precursor. If the t' phase is reduced under a slightly reducing atmosphere even at a sufficiently high temperature for the cationic diffusion, it is inferred that the phase obtained is not a pyrochlore type but a CaF_2-related type or a t' phase; because there is a solubility limit of excess oxygen in the pyrochlore-type $Ce_2Zr_2O_{7+2\delta}$. In contrast, if the t' phase is reduced under strongly reducing atmosphere at a low temperature, it is interesting to find out whether the precursor phase obtained is the CaF_2-related type or the pyrochlore type.

The ordering level between Ce and Zr ions in the κ phase is approximately equivalent to that in the precursor pyrochlore-type phase. The cation-disordered tetragonal phases of t'_{meta}- and t'-$(Ce_{0.5}Zr_{0.5})O_2$ appeared by oxidation of cation-disordered CaF_2-related-type precursors. Because Ce and Zr ions diffuse very slowly through the reoxidation at 873 K, the ordering level between the cations in the precursor phases remains in the reoxidized phases. The oxygen position in the tetragonal phases depends on the temperature for the precursor phase preparation. The origin is still unknown, but the disordering level, i.e., randomness, in the very small region between the cations may influence the oxygen position and the disordering level of cations in the reoxidized phase.

5. CONCLUSIONS

Several cerium zirconium oxides with the composition $CeZrO_4$ were prepared by oxidation of precursor with composition $CeZrO_{3.5+\delta}$ at 873 K. The precursors were obtained by reducing the t'-$(Ce_{0.5}Zr_{0.5})O_2$ at $873 \leq T_{red.} \leq 1573$ K. The structures of the oxidized phase, together with the precursor, were examined as functions of the temperature for precursor preparation, $T_{red.}$. The results obtained are summarized as follows:

(i) The pyrochlore-type precursor $Ce_2Zr_2O_{7+2\delta}$, in which Ce and Zr ions were ordered, was prepared by the reduction of t'-$(Ce_{0.5}Zr_{0.5})O_2$ at $T_{red.} \geq 1323$ K. The ordering level between Ce and Zr ions in the pyrochlore-type precursor decreased with decreasing $T_{red.}$.

(ii) The κ-$CeZrO_4$ phase appeared upon reoxidation of the pyrochlore-type precursor. A completely cation-ordered typical κ-$CeZrO_4$ phase appeared upon reoxidation of the pyrochlore-type precursor with $T_{red.} = 1573$ K. With decreasing $T_{red.}$, the ordering level between Ce^{4+} and Zr^{4+} ions in the κ phase decreased.

(iii) The structural features of the κ-$CeZrO_4$ phase are (a) the cubic system with a space group of $P2_13$, (b) the ordered arrangement between Ce^{4+} and Zr^{4+} ions similar to the pyrochlore-type structure, and (c) the unstable eightfold coordination of Zr^{4+} ions.

(iv) For $T_{red.} \leq 1123$ K, Ce and Zr ions were randomly distributed in the precursors, and the phases were identified as the cubic CaF_2-related phase.

(v) A novel t'-related $(Ce_{0.5}Zr_{0.5})O_2$ phase, which was termed the t'_{meta} phase, and the t'-$(Ce_{0.5}Zr_{0.5})O_2$ phase appeared by reoxidation of the CaF_2-related-type precursor obtained at $T_{red.} = 1123$ and 873 K, respectively.

(vi) The lattice parameters of the t'_{meta}-$(Ce_{0.5}Zr_{0.5})O_2$ phase were smaller than those of the t' phase. The oxygen parameter z of the t'_{meta} phase at the 4*d* site in the space group of $P4_2/nmc$ was estimated to be closer to 0.25 than that of the t' phase. The t'_{meta} phase was more unstable than the t' phase, because the t'_{meta} phase was transformed into the t' phase by heating above 1173 K under the O_2 atmosphere.

(vii) The thermodynamical instability of the κ and t'_{meta} phases, compared with the t' phase, may be due to the ordered arrangement between Zr^{4+} and Ce^{4+} ions and/or the unstable eightfold coordination states of Zr^{4+} ions in these phases.

(viii) The structure of the precursor phases depends on the reduction temperature, time and the reduction ratio, i.e., oxygen content of the precursor. The structure of the reoxidized phases depends on that of the precursor phases. The ordering level between the cations in the precursor phases remains in the reoxidized phases.

ACKNOWLEDGMENTS

The authors thank Santoku Kinzoku Kogyo Co., Ltd., for the supply of CeO_2 and ZrO_2 powders. The authors are grateful for the support in the form of a Grant-in-Aid for Scientific Research from the Ministry of Education, Science, Sports, and Culture (Grant 09555225).

REFERENCES

1. T. Murota, T. Hasegawa, S. Aozasa, H. Matsui, and M. Motoyama, *J. Alloys Comp.* **193,** 298 (1993).
2. M. Ozawa, M. Kimura, and A. Isogai, *J. Alloys Comp.* **193,** 73 (1993).
3. S. Matsumoto, *Toyota Tech. Rev.* **44,** 12 (1994).
4. M. Yashima, K. Morimoto, N. Ishizawa, and M. Yoshimura, *J. Am. Ceram. Soc.* **76,** 1745 (1993).
5. S. Otsuka-Yao, H. Morikawa, N. Izu, and K. Okuda, *J. Jpn. Inst. Met.* **59,** 1237 (1995).
6. S. Otsuka-Yao-Matsuo, T. Omata, N. Izu, and H. Kishimoto, *J. Solid State Chem.* **138,** 47 (1998).
7. S. Otsuka-Yao-Matsuo, N. Izu, T. Omata, and K. Ikeda, *J. Electrochem. Soc.* **145,** 1406 (1998).
8. S. Yao, H. Uchida, and Z. Kozuka, *Mater. Trans. JIM* **31,** 999 (1990).
9. S. Yao, H. Tanaka, and Z. Kozuka, *J. Jpn. Inst. Met.* **55,** 1216 (1991).
10. M. Yashima, H. Arashi, M. Kakihana, and M. Yoshimura, *J. Am. Ceram. Soc.* **77,** 1067 (1994).
11. M. Yashima, K. Ohtake, M. Kakihana, and M. Yoshimura, *J. Am. Ceram. Soc.* **77,** 2773 (1994).
12. N. Izu, T. Omata, and S. Otsuka-Yao-Matsuo, *J. Alloys Comp.* **270,** 107 (1998).
13. T. Uehara, K. Koto, F. Kanamaru, and H. Horiuchi, *Solid State Ionics* **23,** 137 (1987).
14. T. Omata, K. Okuda, S. Tsugimoto, and S. Otsuka-Matsuo-Yao, *Solid State Ionics* **104,** 249 (1997).
15. T. Moriga, A. Yoshiasa, F. Kanamaru, K. Koto, M. Yoshimura, and S. Somiya, *Solid State Ionics* **31,** 319 (1989).
16. T. Moriga, S. Emura, A. Yoshiasa, S. Kikkawa, F. Kanamaru, and K. Koto, *Solid State Ionics* **40/41,** 357 (1990).
17. W. E. Klee and G. Weitz, *J. Inorg. Nucl. Chem.* **31,** 2367 (1969).
18. M. T. Vandenborre, E. Husson, and H. Brusset, *Spectrochim. Acta* **37A,** 113 (1981).
19. M. T. Vandenborre, E. Husson, J. P. Chatry, and D. Michel, *J. Raman Spectrosc.* **14,** 63 (1983).
20. M. T. Vandenborre and E. Husson, *J. Solid State Chem.* **50,** 362 (1983).
21. B. E. Scheetz and W. B. White, *J. Am. Ceram. Soc.* **62,** 468 (1979).
22. N. F. M. Henry and K. Lensalale (Eds.), "Int. Tables for X-ray Crystallography," Vol. I; "Symmetry Groups," Kynoch Press, Birmingham, UK, 1952.
23. J. B. Thomson, A. R. Armstrong, and P. G. Bruce, *Chem. Commun.* 1165 (1996).
24. H. Kishimoto, T. Omata, and S. Otsuka-Yao-Matsuo, in preparation.
25. D. K. Smith and H. W. Newkirk, *Acta Crystallogr.* **18,** 983 (1965).
26. N. Igawa, Y. Ishii, T. Nagasaki, Y. Mori, S. Funahashi, and H. Ono, *J. Am. Ceram. Soc.* **76,** 2673 (1993).
27. M. Yashima, S. Sasaki, M. Kakihana, Y. Yamaguchi, H. Arashi, and M. Yoshimura, *Acta Crystallogr.* **B50,** 663 (1994).
28. U. Martin, H. Boysen, and F. Frey, *Acta Crystallogr.* **B49,** 403 (1993).
29. C. J. Howard, R. J. Hill, and B. E. Reichert, *Acta Crystallogr.* **B44,** 116 (1988).
30. D. N. Argyriou and C. J. Howard, *J. Appl. Crystallogr.* **28,** 206 (1995).
31. B. A. Hunter, C. J. Howard, and D.-J. Kim, *Aust. J. Phys.* **51,** 539 (1998).
32. M. Yashima, T. Hirose, S. Katano, Y. Suzuki, M. Kakihana, and M. Yoshimura, *Phys. Rev.* **B51,** 8018 (1995).
33. M. Yashima, S. Sasaki, Y. Yamaguchi, M. Kakihana, M. Yoshimura, and T. Mori, *Appl. Phys. Lett.* **72,** 182 (1998).